Check for updates

Bimetallic nickel-lutetium complexes: tuning the properties and catalytic hydrogenation activity of the Ni site by varying the Lu coordination environment†

Bianca L. Ramirez, [ID] [a] Prachi Sharma, [ID] [ab] Reed J. Eisenhart,[a] Laura Gagliardi [ID] [ab] and Connie C. Lu [ID] *[a]

We present three heterobimetallic complexes containing an isostructural nickel center and a lutetium ion in varying coordination environments. The bidentate $^iPr_2PCH_2NHPh$ and nonadentate $(^iPr_2PCH_2NHAr)_3tacn$ ligands were used to prepare the Lu metalloligands, $Lu(^iPr_2PCH_2NPh)_3$ (**1**) and $Lu\{(^iPr_2PCH_2NAr)_3tacn\}$ (**2**), respectively. Reaction of $Ni(COD)_2$ (where COD is 1,5-cyclooctadiene) and **1** afforded $NiLu(^iPr_2PCH_2NPh)_3$ (**3**), with a Lu coordination number (CN) of 4 and a Ni–Lu distance, d(Ni–Lu), of 2.4644(2) Å. Complex **3** can further bind THF to form **3-THF**, increasing both the Lu CN to 5 and d(Ni–Lu) to 2.5989(4) Å. On the other hand, incorporation of Ni(0) into **2** provides $NiLu\{(^iPr_2PCH_2NAr)_3tacn\}$ (**4**), in which the Lu coordination environment is more saturated (CN = 6), and the d(Ni–Lu) is substantially elongated at 2.9771(5) Å. Cyclic voltammetry of the three Ni–Lu complexes shows an overall ~410 mV shift in the Ni(0/I) redox couple, suggesting tunability of the Ni electronics across the series. Computational studies reveal polarized bonding interactions between the Ni $3d_{z^2}$ (major) and the Lu $5d_{z^2}$ (minor) orbitals, where the percentage of Lu character increases in the order: **4** (6.0% Lu $5d_{z^2}$) < **3-THF** (8.5%) < **3** (9.3%). All three Ni–Lu complexes bind H_2 at low temperatures (−30 to −80 °C) and are competent catalysts for styrene hydrogenation. Complex **3** outperforms **4** with a four-fold faster rate. Additionally, adding increasing THF equivalents to **3**, which would favor build-up of **3-THF**, decreases the rate. We propose that altering the coordination sphere of the Lu support can influence the resulting properties and catalytic activity of the active Ni(0) metal center.

Introduction

Despite a growing understanding of the chemical bonding between transition metals and 4f elements, the application of d–4f metal interactions in homogeneous catalysis has rarely been studied.[1–3] In contrast, utilization of 4f- and d-block metal cooperativity has proven beneficial in heterogeneous catalysis. For example, lanthanide-based oxide supports have been shown to modify the electronic properties of bulk transition metals in what has been termed as electronic metal-support interactions.[4,5] These electronic perturbations have important ramifications in catalysis, where for example, Pt nanoparticles deposited on a ceria support showed a 20-fold rate enhancement in the water-gas shift reaction compared to Pt(111).[6]

On a related note, 4f-block metal ions that have been incorporated into transition-metal oxide clusters can significantly alter the overall redox potentials and reactivity. For example, a study of $\{LnMn_3O_4\}$ cubanes illustrates that the single Ln ion electronically modulates the Mn_3O_4 cores, where the $\{Ln^{III}Mn_3^{IV}O_4\}/\{LnMn_2^{IV}Mn^{III}O_4\}$ redox couple increases linearly with the pK_a of the $\{Ln^{III}(OH_2)_6\}$ ion, a parameter of Lewis acidity.[7] In a subsequent study on $\{Ln^{III}Co_3^{II}(OAc)_4\}$-cubanes, the single Ln ion serves as an electronic modulator for the cluster and exerts a beneficial effect on the overall photocatalytic water oxidation. The Ln ion boosts the water oxidation activity of the cluster by: (1) increasing the electrochemical driving force, and (2) lowering the energy for acetate–water ligand exchange at the cluster. These effects result in a large increase in the initial rate by two orders of magnitude for $\{LnCo_3(OAc)_4\}$ compared to the tetracobalt cubane, $\{Co_4^{II}(OAc)_4\}$.[8] Of note, in both of these systems, the d and 4f metal centers are separated by bridging oxygen atoms; and hence, these cubanes do not involve any direct d–4f metal

[a]*Department of Chemistry, University of Minnesota, Minneapolis, Minnesota 55455-0431, USA. E-mail: clu@umn.edu*

[b]*Minnesota Supercomputing Institute, Chemical Theory Center, University of Minnesota, Minneapolis, Minnesota 55455-0431, USA*

interactions. Similarly, a heterobimetallic Ni–Nd[III] complex was recently reported where the metal centers are separated via bridging oxygen atoms at a long intermetal distance of 3.505(1) Å, which precludes a direct d–4f interaction.[9]

Expanding on previous work in using direct Ni-group 13 interactions for promoting Ni-mediated H_2/CO_2 catalysis,[10–13] we hypothesized that a direct d–4f metal interaction would allow for a large electronic perturbation of the transition metal, and potentially offer a greater degree of tunability with respect to reactivity. Even so, structural examples of d–4f bonding interactions remain uncommon.[14–23] Selected examples are shown in Fig. 1. To the best of our knowledge, no examples of catalytic reactivity have been reported for any coordination compounds containing a direct d–4f metal interaction. Considering the recent progress in using heterobimetallic metal–metal bonded complexes in catalysis,[24–30] the pursuit of d–4f complexes seemed ripe for exploration. Furthermore, the ability of lanthanides to support a larger range of coordination numbers (CN = 3 to 12)[31] may be advantageous as a new paradigm for tuning catalytic activity. In this case, controlling the supporting Ln ion's coordination environment affords another lever for catalyst tuning.

Two new ligand frameworks were employed to make a triad of heterobimetallic nickel(0)–lutetium(III) complexes, allowing for the first study of nickel-lutetium bonding interactions. The choice of Lu was motivated by the fact that Lu[III] is a diamagnetic ion, which allows for facile characterization by NMR spectroscopy, and that Lu[III] is the most Lewis acidic of the Ln ions, with a pK_a of the {Lu[III]$(OH_2)_6$} ion of 7.9 (cf. pK_a of {La[III]$(OH_2)_6$} is 9.1).[32] Additionally, we show that the electronic properties at Ni are strongly influenced by alteration of the coordination sphere at Lu. The lutetium ion, which acts as a σ-acceptor to Ni, is critical for initiating H_2 binding at the nickel(0) center and its subsequent olefin hydrogenation catalysis. In general, this study probes the effect of tuning the active transition metal beyond its first coordination sphere by altering the coordination environment of the supporting metal.
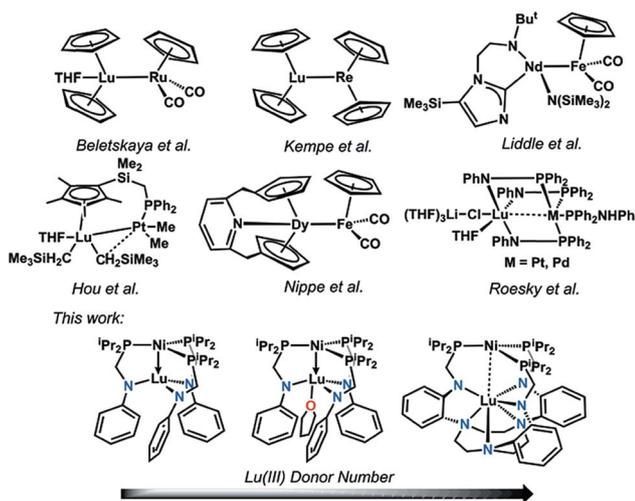

Fig. 1 Selected examples of d–4f heterobimetallic complexes featuring the two metals in close proximity.

Results and discussion

### Preparation of monometallic Lu(III) and bimetallic Ni–Lu compounds

We introduce two ligands, bidentate [i]Pr$_2$PCH$_2$NHPh[33] and nonadentate ([i]Pr$_2$PCH$_2$NHAr)$_3$tacn, which are shown in Scheme 1. Both ligands comprise hard amido and soft phosphine donors. The key step in their syntheses is the condensation reaction of aniline or 1,4,7-tris(2-aminophenyl)-1,4,7-tri-azacyclononane[34] (abbreviated as tacn) with either 1 or 3 equiv. of diisopropylphosphinomethanol, to afford [i]Pr$_2$PCH$_2$NHPh or ([i]Pr$_2$PCH$_2$NHAr)$_3$tacn, respectively.

Deprotonation of [i]Pr$_2$PCH$_2$NHPh (3 equiv.) or ([i]Pr$_2$PCH$_2$-NHAr)$_3$tacn (1 equiv.) with 3 equiv. nBuLi and subsequent addition of $LuCl_3$ afforded the Lu(III) metalloligands, Lu([i]Pr$_2$-PCH$_2$NPh)$_3$ (1) or Lu{([i]Pr$_2$PCH$_2$NAr)$_3$tacn} (2), respectively, as white powders (Scheme 1). Complexes 1 and 2 display a single ^{31}P NMR resonance at −9.4 and −7.1 ppm, respectively, in C_6D_6. These resonances are both shifted upfield from the free ligands, [i]Pr$_2$PCH$_2$NHPh (4.2 ppm) and ([i]Pr$_2$PCH$_2$NHAr)$_3$tacn (3.3 ppm). The ^{1}H-NMR spectrum of 1 shows a single sharp methylene resonance and two nearly coalesced methine resonances, which suggests a nearly ideal C_{3v} solution-state geometry for 1 (Fig. S7†). On the other hand, the ^{1}H-NMR spectrum of 2 has two distinct methine peaks and diastereotopic methylene protons in both the PCH$_2$N and the tacn moieties, which is consistent with C_3 solution-state geometry for 2 (Fig. S8†).

The heterobimetallic Ni–Lu compounds, NiLu([i]Pr$_2$PCH$_2$-NPh)$_3$ (3) and NiLu{([i]Pr$_2$PCH$_2$NAr)$_3$tacn} (4), were isolated from the reaction of Ni(COD)$_2$, where COD = 1,5-cyclooctadiene, with 1 and 2, respectively (Scheme 1). One interesting difference is that the metalation of 1 with Ni(COD)$_2$ gave an immediate color change to dark red, whereas the color of the corresponding reaction with 2 deepened more gradually over several hours to a dark purple-red. Complexes 3 and 4 exhibit a single ^{31}P-NMR resonance at −0.8 and 15.0 ppm, respectively, when in C_6D_6.

During the NMR studies, we uncovered a pronounced solvent effect on the speciation of 3. Upon changing the solvent to THF-d_8, the ^{31}P resonance shifts downfield by 11 ppm. We hypothesized that the THF solvent molecule can coordinate the unsaturated Lu center in 3 to form 3-THF. To interrogate this hypothesis, we sought to first understand the THF-binding equilibrium between 3 and 3-THF. Titrating THF into a toluene-d_8 solution of 3 resulted in the broadening and shifting of a single ^{31}P NMR resonance (Fig. S13,† $\Delta\delta_{max}$ = 11.3). This behavior is consistent with a rapid equilibrium process, where the two species are rapidly interconverting such that only an average signal is observed.[35] Plotting the change in the ^{31}P chemical shift versus THF equivalents yields a hyperbolic binding isotherm that is consistent with a simple equilibrium of 1 : 1 binding.[36] At room temperature, saturation was observed at 80 equiv. of THF (Fig. S12–S14†), and the fitted binding equilibrium constant (K_a) of 59 ± 2 M^{-1},[37,38] which corresponds to ΔG_{298K} = −2.4 kcal mol^{-1}, signifies weak binding of THF to 3.[39,40]
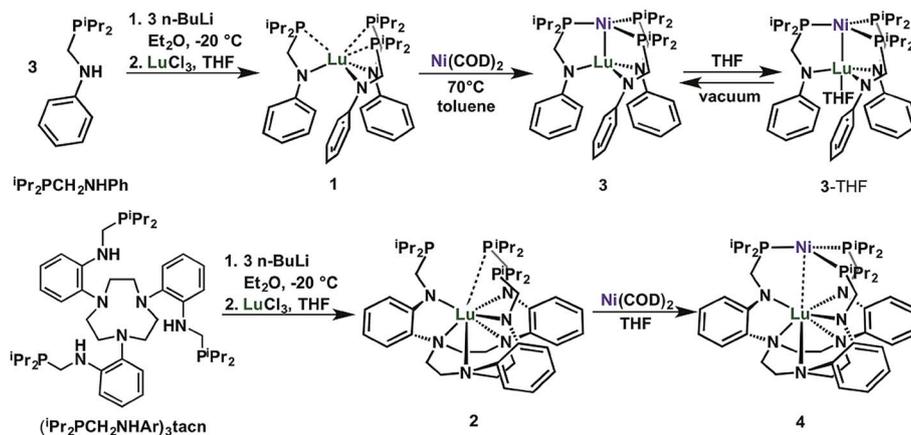
Scheme 1 Synthesis of Lu(III) metalloligands (**1** and **2**) and the corresponding Ni–Lu heterobimetallic complexes (**3**, **3-THF**, and **4**).

On the other hand, **4** showed no notable solvent-dependence of its ^{31}P chemical shift, which is consistent with the Lu site being more fully coordinated and/or sterically protected within the triamido-tacn binding pocket. The ^{1}H-NMR spectra of **3** and **3-THF** are both consistent with an average C_{3v} solution-state geometry, whereas the ^{1}H-NMR spectrum of **4** is indicative of a locked C_3 geometry (Fig. S9–S11†).

Molecular structures of monometallic Lu(III) and bimetallic Ni–Lu compounds

Single-crystal X-ray diffraction studies were performed on **1**, **2**, **3**, **3-THF**, and **4**. The molecular structures are shown in Fig. 2 with average bond distances. Individual bond distances, bond angles, and other relevant geometrical parameters are provided in Table 1. As designed, the two ligand platforms provide different coordination environments for the Lu ion. The molecular structure of **1** reveals a six-coordinate Lu in an N_3P_3-donor environment. The average twist angle (θ) between the P_3- and N_3-triangular faces is 32.6 deg, which is close to the midpoint between an ideal octahedron ($\theta = 60$ deg) and trigonal prism ($\theta = 0$ deg).[41,42]

In **2**, the Lu center is coordinated by six N-donors: three relatively short $Lu–N_{amide}$ bonds of 2.238(5) Å and three slightly longer $Lu–N_{tacn}$ bonds of 2.481(2) Å. The average twist angle of 34.0 deg is also indicative of an intermediate geometry between octahedral and trigonal prismatic. Further, owing to the favoring of high coordination numbers, an additional weak Lu–P interaction with a distance of 3.2451(9) Å was observed in the molecular structure of **2**. The two Lu metalloligands also differ in the position of the Lu center relative to the triamido donor set, which will be referred to as forming the N_3-plane. In **1**, Lu resides in between the P_3- and N_3-planes at ~0.8 Å "above" the
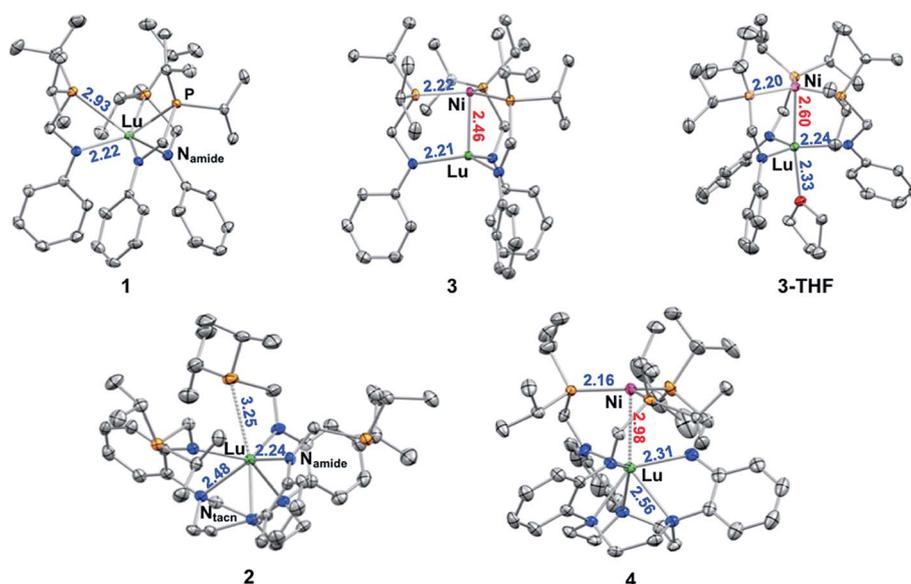

Fig. 2 Molecular structures of **1–4** shown at 50% thermal ellipsoid probability. Hydrogen atoms and non-coordinating solvent molecules have been omitted for clarity. The average bond lengths (Å) are shown. Atom colors: Lu, green; Ni, pink; P, orange; N, blue; O, red; C, gray.

Table 1 Geometrical parameters, including bond lengths (Å) and angles (deg), for **1**–**4**[a]

	1	**2**	**3**	**3-THF**	**4**
Ni–Lu	—	—	2.4644(2)	2.5989(4)	2.9771(5)
Ni–P	—	—	2.2078(4), 2.2211(4), 2.2275(4)	2.1834(8), 2.2046(9), 2.2121(8)	2.1576(8), 2.1643(9), 2.1682(15)
Avg. Ni–P	—	—	2.2188(2)	2.2000(5)	2.1634(6)
Lu–P	2.8873(6), 2.9398(6), 2.9536(6)	3.2451(9)	—	—	—
Avg. Lu–P	2.9269(3)	—	—	—	—
Lu–N$_{amide}$	2.2207(17), 2.2233(19), 2.2251(17)	2.210(3), 2.251(3), 2.252(3)	2.2037(12) 2.2132(11) 2.2211(11)	2.1834(8), 2.2046(9), 2.2121(8)	2.298(2) 2.299(3) 2.324(2)
Avg. Lu–N$_{amide}$	2.223(1)	2.238(1)	2.213(1)	2.200(1)	2.307(1)
P–Ni–P	—	—	121.133(15), 118.340(15), 119.928(15)	121.99(3), 118.62(3), 118.58(3)	120.26(3), 116.03(5), 122.35(5)
$\sum$(P–Ni–P)	—	—	359.401(3)	359.19(5)	358.64(8)
N$_{amide}$–Lu–N$_{amide}$	109.79(7), 108.75(6), 105.39(6)	103.37(10) 106.64(10), 126.55(9)	115.88(4), 118.47(4), 118.04(5)	112.32(9), 114.48(9), 133.20(9)	116.29(8), 119.31(9), 113.10(9)
$\sum$(N$_{amide}$–Lu–N$_{amide}$)	323.93(11)	336.56(17)	352.39(8)	360.00(16)	348.69(15)
Lu–N$_{tacn}$	—	2.445(3), 2.495(3), 2.502(3)	—	—	2.559(2), 2.563(2), 2.563(2)
Avg. Lu–N$_{tacn}$	—	2.481(2)	—	—	2.562(1)
Lu to N$_3$-plane	0.7935(10)	−0.6281(16)	0.3559(7)	0.0090(13)	−0.4533(14)
Ni to P$_3$-plane	—	—	0.0995(3)	0.1150(6)	0.1464(8)

[a] Estimated standard deviations (esd's) are provided in parentheses.

N$_3$-plane. On the other hand, Lu resides ∼0.6 Å "below" the N$_3$-plane in **2**.

The three Ni–Lu bimetallic complexes, **3**, **3-THF**, and **4**, each have a common NiP$_3$ site, but a different Lu geometry and coordination number (CN). In **3** and **3-THF**, the Lu geometry is trigonal pyramidal (CN = 4) and trigonal bipyramidal (CN = 5, τ_5 = 0.66), respectively.[43] In **4**, the Lu geometry is intermediate between octahedral and trigonal prismatic (CN = 6, θ = 35.6 deg). The Ni–Lu bond distance also varies significantly across the triad. Interestingly, the coordination environment of the Lu appears to dictate the proximity between Ni and Lu. For example, complex **3** possesses the lowest coordinate Lu in this series and has the shortest Ni–Lu bond distance of 2.4644(2) Å. In **3-THF**, the addition of a single THF donor along the metal–metal axis increases the CN of Lu by 1 and elongates the Ni–Lu bond distance by 0.14 Å to 2.5989(4) Å. In **4**, the 6-coordinate Lu center is either non- or only weakly bonding to Ni with a long Ni–Lu distance of 2.9771(5) Å, which is longer than that in **3** by over 0.5 Å.

Complexes **3**, **3-THF**, and **4** join a handful of crystallographically characterized compounds containing both Ni and Lu metals. Among these examples, the intermetal distances are too large to allow for any significant metal–metal interactions.[44–50] Hence, without sufficient experimental comparisons to evaluate and/or interpret our Ni–Lu bond distances, we considered several different approaches for estimating a single bond length that is based on summing the two atoms' radii. Depending on the radii values, predictions of a single bond length can vary. Pyykkö and Atsumi derived a self-consistent system of single-bond covalent radii based on both experimental and theoretical data.[51,52] Covalent radii have also been

tabulated by Cordero and co-workers using a large data set obtained from the Cambridge Structural Database.[53] Another complementary set of values are Pauling's single-bond metallic radii.[54] Using the above approaches, the predicted distances of a single Ni–Lu covalent bond are: 2.72 Å (Pyykkö and Atsumi), 3.11 Å (Cordero et al.), and 2.706 Å (Pauling). Compared with these estimates, the Ni–Lu bond lengths in **3** (2.46 Å) and **3-THF** (2.60 Å) are significantly shorter. Of note, the shortest Ni–Lu bond distances that were previously reported are in the range of 2.92 to 3.15 Å (Table S2†).[44,48] Hence, we conclude that the Ni–Lu bond lengths in both **3** and **3-THF** are consistent with direct Ni–Lu bonding interactions.

Notably, the intermetallic bond distance in **3** is significantly shorter than that of any other d–f bimetallic compound that has been crystallographically characterized (Table S2†). Prior to this work, the shortest d–f bond length of 2.520(1) Å was reported for NiUF(2-PPh$_2$-4-Me-6-tBu(C$_6$H$_2$O))$_3$.[55] If one accounts for the single-bond covalent radius difference between Lu (1.62 Å) and U (1.70 Å), then **3** and NiUF(2-PPh$_2$-4-Me-6-tBu(C$_6$H$_2$O))$_3$ have similar r values of 0.91 and 0.90, respectively, where r is the ratio of their metal–metal bond distance to the corresponding sum of the metals' single-bond radii.[51] Also, only a handful of Lu-group 10 compounds have been reported that have intermetal distances < 3 Å.[15,44,56,57] These limited examples include (C$_5$Me$_4$SiMe$_2$CH$_2$PPh$_2$)Lu(μ-CH$_2$SiMe$_2$CH$_2$)(OC$_4$H$_8$)PtMe$_2$ and [(Ph$_2$PNHPh)M{μ-(Ph$_2$PNPh)}$_3$Lu(μ-Cl)Li(THF)$_3$] (M = Pd or Pt), where the intermetallic distances are longer at 2.7668(5) Å, 2.9031(11), and 2.9523(9), respectively.

Comparing **3**, **3-THF**, and **4**, the Lu–N$_{amide}$ bond length elongates with increasing CN. In both ligand systems, the Lu ion becomes increasingly co-planar with the triamido donors upon

incorporating Ni into the metalloligand. The distance between Lu and the N_3-plane also correlates well with the Ni–Lu distance. In **3**, Lu is 0.4 Å above the N_3-plane and closest to Ni. In **3-THF**, Lu is nearly co-planar with a slightly longer Ni–Lu distance. In contrast, Lu is positioned below the N_3-plane by 0.5 Å in **4**, which is consistent with little or no interaction with Ni. On the other hand, the Ni site is relatively invariant across **3**, **3-THF**, and **4**, where the distance between Ni and the P_3-plane only changes slightly, from 0.10 to 0.15 Å. The only notable difference in the Ni coordination sphere is the contraction of the Ni–P bonds from **3** (avg. 2.22 Å) to **3-THF** (2.20 Å) to **4** (2.16 Å). This trend is consistent with increased π-back-bonding from a more electron-rich Ni center in **4** (relative to **3** and **3-THF**) to the phosphine ligands. The greater Ni electron density in **4** further suggests diminished Lewis acidity of Lu(III), which can be rationalized by the longer Ni–Lu distance and the increase in the Lu(III) coordination environment.

Electrochemistry

To probe the influence of the Lu(III) metalloligand on the electronics at the Ni center, cyclic voltammetry experiments were performed. Fig. 3 is an overlay of the cyclic voltammograms (CVs) of **3**, **3-THF**, and **4**. The CVs were collected in 0.1 M $[^nPr_4N][BAr^F_4]$ electrolyte solutions (Ar^F = 3,5-bis(trifluoromethyl)phenyl) and internally referenced to the $[FeCp_2]^{+/0}$ potential. Because coordinating solvents can bind an unsaturated Lu(III) center, the electrochemical study of **3** was performed in 1,2-difluorobenzene (DFB).[58] To minimize any shifts in the $[FeCp_2]^{+/0}$ reference potential due to solvent effects,[59] the CV of **4** was also measured in DFB. For the CV study of **3-THF**, the sample was prepared by adding 320 equiv. THF to **3** in DFB. For both **3-THF** and **4**, the CVs were also collected in THF.

In DFB, **4** displayed a reversible Ni(0/I) oxidation at $E_{1/2}$ = −1.41 V vs. $[FeCp_2]^{+/0}$ (Fig. 3).[12] Complex **3** showed an irreversible oxidation at E_{pa} = −1.00 V in DFB, which is ~410 mV more positive than that of **4**. In situ generation of **3-THF** results in
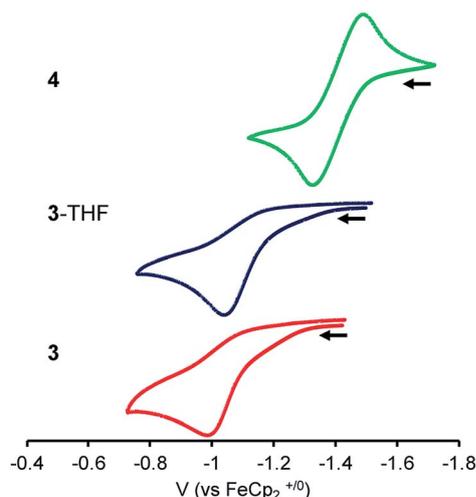

Fig. 3 CVs of **3**, **3-THF** and **4** with 0.1 M $[^nPr_4N][BAr^F_4]$ electrolyte in DFB (scan rate of 100 mV s^{-1}; collected under Ar).

a ~50 mV cathodic shift in the irreversible oxidation to E_{pa} = −1.05 V (Fig. 3 and S42†). In THF, the Ni(0/I) oxidation for **3-THF** becomes quasi-reversible at E_{pa} = −0.97 V (i_{pc}/i_{pa} = 0.6 at 250 mV s^{-1}, Fig. S43†). The Ni(0/I) redox couple for **4** remains reversible in THF, with $E_{1/2}$ = −1.44 V (Fig. S45†). Of note, the Ni(0/I) redox potential for **3-THF** is 470 mV more positive than that of **4** in THF, whereas the difference in their redox potentials decreases to ~360 mV in DFB.

Overall, the Ni(0/I) oxidation potential becomes increasingly positive in moving from **4** to **3-THF** to **3**. This trend correlates with the increasing strength of the Ni–Lu interaction, as reflected by the intermetal distances. Hence, the Ni(0) center in **3** shows the greatest withdrawal of electron density, or alternatively, the Lu(III) support in **3** exhibits the greatest Lewis acidity in this series. This supports the hypothesis that the less coordinatively saturated Lu(III) supporting ion more greatly perturbs the Ni electronics, presumably via better bonding overlap with the soft Ni(0) Lewis base. Because the Ni–Lu interaction is greatly attenuated in **4**, the Ni electronics may be expected to resemble that of the mononickel complex, $Ni\{N(o-(NCH_2P^iPr_2)C_6H_4)_3\}$,[60] which has an isostructural Ni(0) center within a tris(diisopropylphosphine) coordination environment. The mononickel complex displays a reversible Ni(0/I) redox couple at $E_{1/2}$ = −1.26 V in 0.1 M $[^nPr_4N][BAr^F_4]$/DFB (Fig. S46†), signifying that **4** is slightly more electron-rich than $Ni\{N(o-(NCH_2P^iPr_2)C_6H_4)_3\}$.

As an aside, an irreversible reduction at E_{pc} ~ −3 V was also observed for **3-THF** in 0.1 M $[^nBu_4N][PF_6]$/THF, whereas no reduction events are observed for **4** in the same electrolyte solution (Fig. S47†). So far, no reduction process has been observed for **3**. However, this may be due to the more limited electrochemical window of DFB, for which we measured a lower limit of −2.8 V vs. $[FeCp_2]^{+/0}$ (Fig. S52†).

Electronic absorption spectroscopy

The colors of the Ni–Lu complexes are varying shades of red: bright red for **3**, red orange for **3-THF**, and purple red for **4**. Fig. 4 shows an overlay of the UV-vis spectra for the Ni–Lu complexes. Compound **4** displays an intense band at 504 nm (ε = 4700 M^{-1} cm^{-1}). A similar absorption was observed for the mononickel compound, $Ni\{N(o-(NCH_2P^iPr_2)C_6H_4)_3\}$ (cf. 491 nm, ε = 4300 M^{-1} cm^{-1}).[60] The striking similarity between **4** and $Ni\{N(o-(NHCH_2P^iPr_2)C_6H_4)_3\}$ also suggests that the Lu(III) ion minimally perturbs the Ni electronics in **4**.

Complexes **3** and **3-THF** each display two overlapping bands in the region from 370 to 420 nm, and a third low-intensity absorption at higher wavelengths of 515 and 550 nm, respectively (Fig. 4, S50 and S51†). Both spectra qualitatively resemble that reported for $NiAl\{N(o-(NCH_2P^iPr_2)C_6H_4)_3\}$, which contains a dative Ni → Al bonding interaction.[61] Hence, we propose that the stark change in the UV-vis spectrum of **4** and that of **3** or **3-THF** is consistent with the presence of Ni → Lu bonding interactions in both **3** and **3-THF**.

Computational investigation of 3, 3-THF, and 4

To investigate the electronic structures of **3**, **3-THF**, and **4** and to better understand the nature of their metal–metal interactions,
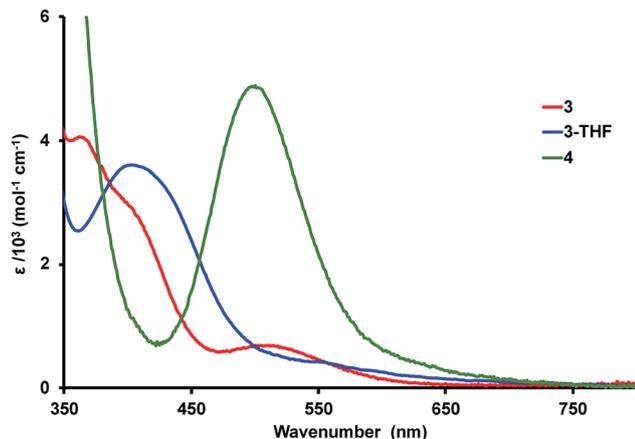
Fig. 4 UV-vis spectra of complexes **3** (red) and **4** (green) in DFB and **3-THF** (blue) in THF at 298 K.

we performed quantum-chemical calculations on the full structures. Geometry optimizations were conducted using density functional theory (DFT) at PBE-D3 [62–64] level of theory, and the optimized ground-state geometries compare well to the experimental structures (Table S7†). For further studies, complete active-space self-consistent field (CASSCF)[65] calculations were performed. For each Ni–Lu complex, the active natural orbitals included five Ni 3d orbitals that are each doubly occupied. Notably, one of the orbitals, though heavily Ni based (*ca.* 90% or greater), showed non-negligible contributions from Lu (Fig. 5, S52–S54†). This natural orbital revealed a polarized bonding interaction between the Ni $3d_{z^2}$ and the Lu $5d_{z^2}$, where the percentage of Lu character increases slightly in the order: **4** (6.0% Lu $5d_{z^2}$) < **3-THF** (8.5%) < **3** (9.3%) (Table S9†). The trend is consistent with the increasing proximity of the Ni and Lu centers and with a lower coordination number for Lu, both of which would result in better bonding overlap between these two metals. The large degree of polarization in this natural orbital further suggests that the Ni–Lu bonding is best described as a dative interaction of the Ni $3d_{z^2}$ electrons into the empty Lu $5d_{z^2}$ orbital.

The molecular orbital (MO) diagrams for **3**, **3-THF**, and **4**, which were obtained from DFT calculations, are shown in Fig. 6 (Fig. S55–S57†). In comparing **3** and **4**, the different Lu supports have a profound effect on the relative energy of the Ni $3d_{z^2}$ orbital. For **4**, the Ni $3d_{z^2}$ orbital is more destabilized than the Ni $3d_{xz}/3d_{yz}$ orbitals and is stabilized relative to the Ni $3d_{x^2-y^2}/3d_{xy}$ orbitals, as one would expect for a metal center with trigonal donors. For both **3** and **3-THF**, the Ni $3d_{z^2}$ orbital is the most energy-stabilized Ni d-orbital, presumably due to Ni $3d_{z^2}$ → Lu $5d_{z^2}$ interaction. Also of note, the LUMO for all the Ni–Lu bimetallic complexes is primarily comprised of the Ni $4p_Z$ and Lu $6s/5d_{z^2}$ orbitals, with additional contribution from the P $3p_Z$ orbitals (Table S13†). The presence of an energetically accessible metal-based $4p_Z$ LUMO has also been invoked in other
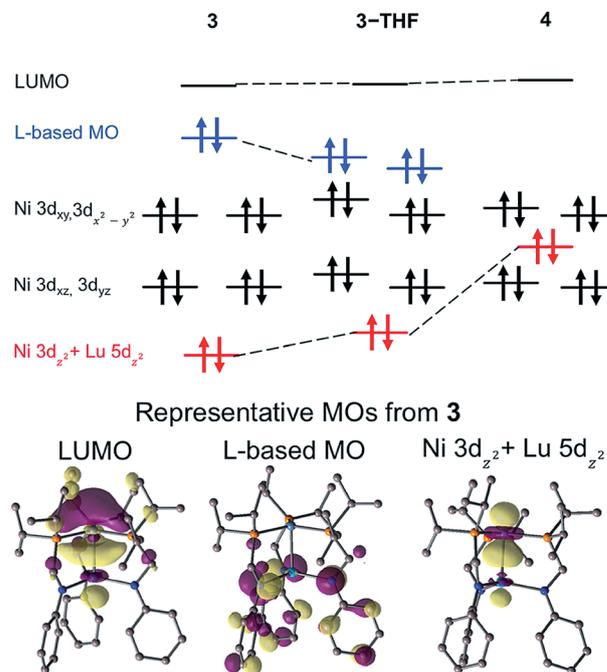

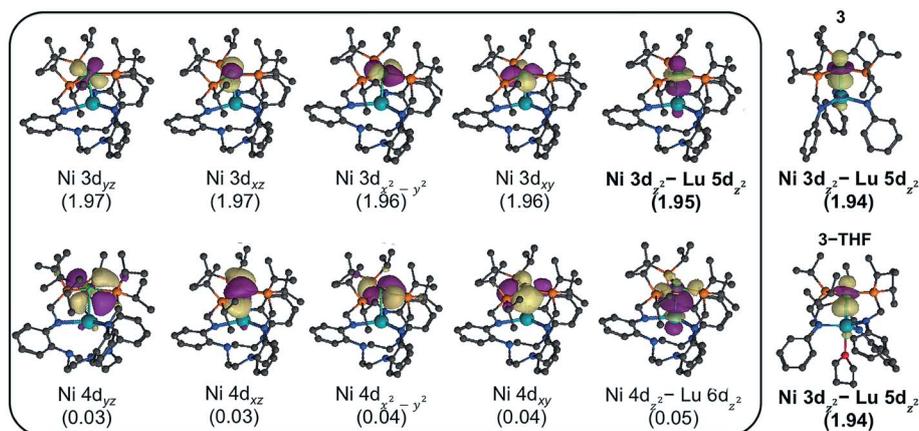Fig. 6 DFT-derived qualitative MO diagrams across the Ni–Lu series.

Fig. 5 CASSCF-derived natural orbitals for **4**, shown with occupation numbers. Similar natural orbitals were observed for **3** and **3-THF**. Shown to the right, the Ni $3d_{z^2}$ natural orbitals for **3** and **3-THF**, where a minor contribution from Lu $5d_{z^2}$ is visible.

transition metal-group 13 coordination complexes.[28,66,67] Binding of weak sigma donors, ranging from solvent donors[67] to H_2[11,12,68,69] have been reported, which can be attributed to the energetically low-lying, metal-based $4p_Z$ acceptor orbital.[70] Hence, the prediction of similar LUMOs in each of the Ni–Lu bimetallic complexes may also indicate that their respective Ni sites are primed to bind H_2.

H_2 reactivity and catalysis

Compounds **3**, **3-THF**, and **4** showcase a range of H_2 binding reactivity. At ambient temperature and 1 atm H_2, none of these complexes showed any formation of the Ni(η^2-H_2) adducts.[12] However, the ^{31}P peak of the bimetallic compounds and the ^1H signal for free H_2 both shifted slightly, which could be a hint of weak binding (Fig. S16–S23†). Hence, to maximize H_2 binding, samples of **3-THF** and **4** in THF-d_8 were subjected to 4 atm H_2 (at room temperature) and characterized *in situ* by low-temperature NMR spectroscopy. To study H_2 binding to **3**, the same protocol was applied except that toluene-d_8 was used as the solvent. The low-temperature NMR spectra for **3** have notably weaker signal intensities due to its poor solubility in non-coordinating solvents.

At −80 °C and 4 atm H_2, an equilibrium between **3** and a new species was observed in an approximately 1 : 0.4 ratio based on the appearance of two ^{31}P peaks at −1.7 and 9.6 ppm, respectively (Fig. S24 and S25†). The assignment of the new species as the η^2-H_2 adduct, **3**-(H_2), is based on the appearance of a broad ^1H resonance at −1.4 ppm (Fig. S26†). T_1 (min) relaxation time measurements, however, could not be obtained due to the broadness of the resonance. At −80 °C and 4 atm H_2 in THF-d_8, a similar equilibrium between **3-THF** and a new species was observed in an approximate 1 : 2.5 ratio based on the appearance of two ^{31}P peaks at 8.9 and 22.5 ppm, respectively (Fig. S29 and S30†). The assignment of the new species as the η^2-H_2 adduct, **3**(H_2)–**THF**, is based on the appearance of a broad ^1H resonance at −1.3 ppm (Fig. S31†), whose short T_1(min) relaxation time of 20(1) ms (400 MHz) is consistent with an intact H_2 ligand (Fig. S33†).[71] On the other hand, exposing **4** to 4 atm H_2 at −80 °C (in either THF–d_8 or toluene-d_8) did not generate an

observable H_2 adduct, though broadening in the ^{31}P resonance and the disappearance of the free H_2 resonance both suggest that **4** does interact with H_2, even if weakly (Fig. S34 and S35†). Hence, the strength of the H_2 interaction with the Ni(0) center decreases in the order, **3-THF** > **3** ≫ **4**. Moreover, the *in situ* characterization of **3**-(H_2)THF adds to the few (η^2-H_2)Ni(0) examples in the literature.[11,12] Since the Ni center is more electron-deficient in both **3-THF** and **3** than in **4**, the Ni–Lu compounds roughly follow the same trend that was observed previously for bimetallic Ni-group 13 complexes.[12,28] Namely, the more Lewis acidic metalloligands lead to more stable Ni(η^2-H_2) adducts.

Following the H_2 binding studies, we investigated the propensity of **3** and **4** to mediate catalytic olefin hydrogenation, a process which is typically challenging for a single Ni center to perform.[10,12,68,72–79] In general, the greater lack of molecular Ni hydrogenation catalysts compared to related first–row transitions metals such as Fe and Co may be attributed to the greater electronegativity of Ni, which would hinder π-backbonding and consequently, H_2 activation.[80] Using a loading of 2.5 mol%, **3** catalyzes the hydrogenation of styrene to ethyl benzene in high yield under 4 atm H_2 and heating at 100 °C in toluene-d_8 for 2 h (Table 2, entry 1). Under these standard conditions, **4** also performs the catalysis, albeit more sluggishly and in low yield (entry 2). The importance of the Lu supporting ion can be inferred from the monometallic Ni control reactions (entries 3–5), where neither the mononickel complex, Ni{N(o-(NCH$_2$P^{i}Pr$_2$) C$_6$H$_4$)$_3$}, nor the catalyst mixtures of Ni(COD)$_2$ with either of the current ligands gave any significant product. Further, the Lu metalloligands (**1** and **2**) by themselves do not mediate this catalysis (Table S4†). Finally, the presence of excess Hg during catalysis did not affect the turnovers achieved by either **3** or **4**, which supports their homogeneous nature (see ESI†).

We also sought to investigate the effect of THF binding to the remote Lu site on the hydrogenation of styrene. If the reaction solvent is changed to THF (and consequently, a lower reaction temperature of 63 °C), then the overall rate of catalysis diminishes by nearly three-fold between **3** and **3-THF** (entries 6 and 7). However, the addition of less than 40 equiv. THF has no

Table 2 Hydrogenation of styrene to ethylbenzene mediated by **3** and **4**[a]

Entry	Catalyst	T (°C)	% Conversion	Overall rate (h^{-1})
1	**3**	100	94(4)[c]	18.8(9)
2	**4**	100	24(3)[c]	4.7(2)
3	Ni{N(o-(NCH$_2$P^{i}Pr$_2$)C$_6$H$_4$)$_3$}	100	<1[c]	0
4	Ni(COD)$_2$ + 3 equiv. ^{i}Pr$_2$PCH$_2$NHPh	100	8(1)[c]	1.6(2)
5	Ni(COD)$_2$ + (^{i}Pr$_2$PCH$_2$NHAr)$_3$tacn	100	<1[c]	0
6	**3**	63	>99[d]	4.1(1)
7[b]	**3-THF**	63	35(2)[d]	1.4(1)
8	**3** + 20 equiv. THF	63	96(1)[d]	3.9(1)
9	**3** + 40 equiv. THF	63	86(2)[d]	3.5(1)
10	**3** + 110 equiv. THF	63	77(1)[d]	3.1(1)
11	**3** + 660 equiv. THF	63	68(3)[d]	2.7(1)

[a] Catalytic conditions: 2.5 mol% catalyst, 0.37 M olefin in *ca.* 600 μL of d_8-toluene, 4 atm H_2. Conversion are based on triplicate runs using ^1H NMR integration. [b] In *ca.* 600 μL of d_8-THF. [c] t = 2 h. [d] t = 10 h.

observable effects on the rate. Above 40 equiv. THF, the rate perceptibly decreases with increasing THF equivalents. Presumably, the negligible changes in rate at lower concentrations of THF is due to its weak reversible binding at the Lu^{III} center of **3** at 63 °C such that solvent effects are only manifested at higher concentrations. Indeed, the effect of THF on the rate of catalysis highlights the remote binding effect of THF on **3** and, in turn, the importance of the lanthanide coordination environment in the design of future d–f-bonded heterometallic catalysts.

Lastly, the substrate scope was further investigated for catalyst **3** (Table S5,† % conversion at 24 h). Under the standard catalytic conditions, **3** readily hydrogenated unhindered alkenes (>99%), including terminal and cyclic olefins: 1-octene, allylbenzene, and *cis*-cyclooctene. Linear internal olefins were either hydrogenated more sluggishly, *e.g. trans*-2-octene (68%), or were unreactive (<2%), *e.g. trans*-4-octene and *trans*-stilbene. For *cis*-stilbene, facile isomerization to the thermodynamically favored *trans*-stilbene was observed (93%) with some bibenzyl formation (7%). In the absence of H$_2$, only a small amount of isomerization (7%) was observed even after 26 h, which demonstrates the importance of H$_2$ for the isomerization reaction. Overall, the substrate scope for **3** is similar to that reported for a similar Ni–Ga complex.[12] One surprising difference is the different outcomes with allylbenzene: **3** generated propylbenzene in nearly quantitative yield in 2 h, whereas reaction with the Ni–Ga catalyst only showed 3% yield at 24 h. Perhaps, the greater flexibility of the non-tethered ligand of **3** allows for its greater reactivity with this substrate.

Conclusions

This work studies the effect of tuning an active metal (Ni) beyond its primary coordination sphere, specifically by tuning the ligand environment of a supporting Lewis acidic ion (Lu). Through the employment of two new phosphinoamido ligand frameworks, **1** and **2**, three new heterobimetallic Ni(0)-Lu(III) complexes were synthesized. The ligand [^{i}Pr$_2$PCH$_2$NPh]$^-$ stabilizes the Ni–Lu complex, **3**, with a low-coordinate Lu ion (CN = 4), and the Ni–Lu interaction exists without any competing *trans*-ligand(s). The Ni–Lu interaction can be perturbed simply by the addition of THF, which binds reversibly to the Lu center in **3-THF** (CN = 5). At the other extreme, the [[^{i}Pr$_2$PCH$_2$NAr]$_3$-**tacn**]$^{3-}$ ligand enforces a more saturated Lu environment (CN = 6), resulting in a diminished Ni–Lu interaction in **4**. This work showcases the first two examples of coordination complexes with Ni–Lu bonding interactions, which also collectively add to the few examples of complexes with direct 3d–4f interactions.

Varying the coordination environment of the distal Lu ion significantly impacts the ability of Lu to act as a Lewis acidic acceptor for the Ni metal, which consequently, impacts the Ni–Lu bonding interaction. Changes in the latter are reflected in the Ni–Lu distances differing by over 0.5 Å, as well as the variable mixing of the Lu and Ni d$_{z^2}$ orbitals in the σ-bonding MO. We propose that the different Ni–Lu bonding interactions are the underlying reason for the property and reactivity differences among these otherwise isostructural Ni sites. For example,

tunability of the Ni electronics across the series is reflected in the ~410 mV shift in the Ni(0/I) oxidation potential. Large variability in H$_2$ binding is also evident: while barely detectable for **4**, Ni(η^2-H$_2$) adducts are spectroscopically characterized at low *T* for both **3** and **3-THF**. To our knowledge, the latter are the first reported non-classical H$_2$ adducts for any d–f hetero-bimetallic compounds, and they represent the first demonstration of using Ln supports to induce H$_2$ binding at a single Ni center.

The accumulation of these remote coordination effects on the Ni electronics further influences their catalytic activity. Complex **3** outperforms **4** in catalytic styrene hydrogenation by a factor of 4. Further, the presence of an open coordination site at Lu in **3** presents the unique opportunity to tune catalytic activity *via* external ligand binding at this remote site. Along these lines, adding increasing equivalents of THF to **3** does decrease the overall rate of hydrogenation, albeit more than 40 equiv. of THF are necessary to impede the rate.

In closing, d–f bonding interactions appear promising for promoting reactivity at a base transition metal center. From the perspective of catalyst design, lanthanide supporting ions may offer key advantages. The full Ln series is synthetically accessible for fine tuning of both the Lewis acidity and ionic size of the supporting 4f ion. Developing low-coordinate Ln metalloligands that allow for dynamic binding of external ligands may also be potentially useful for switchable catalysis applications, and as a general design strategy for tuning beyond the binding site. We are currently exploring these research avenues.

Conflicts of interest

There are no conflicts of interest.

Acknowledgements

References

1 M. V. Butovskii and R. Kempe, *New J. Chem.*, 2015, **39**, 7544–7558.

2 B. Oelkers and R. Kempe, in *Molecular Metal-Metal Bonds*, Wiley-VCH Verlag GmbH & Co. KGaA, Weinheim, 1st edn, 2015, pp. 47–71.

3 S. T. Liddle and D. P. Mills, *Dalton Trans.*, 2009, 5592–5605.

4 C. T. Campbell, *Nat. Chem.*, 2012, **4**, 597–598.

5 M. Ahmadi, H. Mistry and B. Roldan Cuenya, *J. Phys. Chem. Lett.*, 2016, **7**, 3519–3533.

6 A. Bruix, J. A. Rodriguez, P. J. Ramírez, S. D. Senanayake, J. Evans, J. B. Park, D. Stacchiola, P. Liu, J. Hrbek and F. Illas, *J. Am. Chem. Soc.*, 2012, **134**, 8968–8974.

7 P.-H. Lin, M. K. Takase and T. Agapie, *Inorg. Chem.*, 2015, **54**, 59–64.

8 F. Evangelisti, R. Moré, F. Hodel, S. Luber and G. R. Patzke, *J. Am. Chem. Soc.*, 2015, **137**, 11076–11084.

9 A. Kumar, D. Lionetti, V. W. Day and J. D. Blakemore, *Chem.–Eur. J.*, 2018, **24**, 141–149.

10 W. H. Harman and J. C. Peters, *J. Am. Chem. Soc.*, 2012, **134**, 5080–5082.

11 W. H. Harman, T.-P. Lin and J. C. Peters, *Angew. Chem., Int. Ed.*, 2014, **53**, 1081–1086.

12 R. C. Cammarota and C. C. Lu, *J. Am. Chem. Soc.*, 2015, **137**, 12486–12489.

13 R. C. Cammarota, M. V. Vollmer, J. Xie, J. Ye, J. C. Linehan, S. A. Burgess, A. M. Appel, L. Gagliardi and C. C. Lu, *J. Am. Chem. Soc.*, 2017, **139**, 14244–14250.

14 I. P. Beletskaya, A. Z. Voskoboynikov, E. B. Chuklanova, N. I. Kirillova, A. K. Shestakova, I. N. Parshina, A. I. Gusev and G. K. I. Magomedov, *J. Am. Chem. Soc.*, 1993, **115**, 3156–3166.

15 Y. Nakajima and Z. Hou, *Organometallics*, 2009, **28**, 6861–6870.

16 M. V. Butovskii, C. Döring, V. Bezugly, F. R. Wagner, Y. Grin and R. Kempe, *Nat. Chem.*, 2010, **2**, 741–744.

17 M. V. Butovskii, O. L. Tok, V. Bezugly, F. R. Wagner and R. Kempe, *Angew. Chem., Int. Ed.*, 2011, **50**, 7695–7698.

18 M. V. Butovskii, O. L. Tok, F. R. Wagner and R. Kempe, *Angew. Chem., Int. Ed.*, 2008, **47**, 6469–6472.

19 C. Döring, A. M. Dietel, M. V. Butovskii, V. Bezugly, F. R. Wagner and R. Kempe, *Chem.–Eur. J.*, 2010, **16**, 10679–10683.

20 A. Spannenberg, M. Oberthür, H. Noss, A. Tillack, P. Arndt and R. Kempe, *Angew. Chem., Int. Ed.*, 1998, **37**, 2079–2082.

21 P. L. Arnold, J. McMaster and S. T. Liddle, *Chem. Commun.*, 2009, 818–820.

22 C. P. Burns, X. Yang, J. D. Wofford, N. S. Bhuvanesh, M. B. Hall and M. Nippe, *Angew. Chem., Int. Ed.*, 2018, **57**, 8144–8148.

23 C. P. Burns, X. Yang, S. Sung, J. D. Wofford, N. S. Bhuvanesh, M. B. Hall and M. Nippe, *Chem. Commun.*, 2018, **54**, 10893–10896.

24 B. G. Cooper, J. W. Napoline and C. M. Thomas, *Catal. Rev.*, 2012, **54**, 1–40.

25 P. Buchwalter, J. Rosé and P. Braunstein, *Chem. Rev.*, 2015, **115**, 28–126.

26 D. R. Pye and N. P. Mankad, *Chem. Sci.*, 2017, **8**, 1705–1718.

27 I. G. Powers and C. Uyeda, *ACS Catal.*, 2017, **7**, 936–958.

28 R. C. Cammarota, L. J. Clouston and C. C. Lu, *Coord. Chem. Rev.*, 2017, **334**, 100–111.

29 N. P. Mankad, *Chem.–Eur. J.*, 2016, **22**, 5822–5829.

30 C. M. Thomas, *Comments Inorg. Chem.*, 2011, **32**, 14–38.

31 C. Huang and Z. Bian, in *Rare Earth Coordination Chemistry*, ed. C. Huang, John Wiley & Sons, Singapore, 1st edn, 2010, pp. 1–40.

32 D. D. Perrin, *Ionisation Constants of Inorganic Acids and Bases in Aqueous Solution*, ed. D. D. Perrin, Pergamon, Oxford, 2nd edn, 1982, pp. 1–138.

33 E. Payet, A. Auffrant, X. F. Le Goff and P. L. Floch, *J. Organomet. Chem.*, 2010, **695**, 1499–1506.

34 I. A. Fallis, R. D. Farley, K. M. A. Malik, D. M. Murphy and H. J. Smith, *J. Chem. Soc., Dalton Trans.*, 2000, 3632–3639, DOI: 10.1039/b005402j.

35 I. R. Kleckner and M. P. Foster, *Biochim. Biophys. Acta, Proteins Proteomics*, 2011, **1814**, 942–968.

36 J. Kuriyan, B. Konforti and D. Wemmer, in *The Molecules of Life: Physical and Chemical Properties*, Garland Publishing, New York, 1st edn, 2013, pp. 531–580.

37 P. Thordarson, Supramolecular.org, http://supramolecular.org/, accessed July 13, 2018.

38 D. Brynn Hibbert and P. Thordarson, *Chem. Commun.*, 2016, **52**, 12792–12805.

39 L. Fielding, *Tetrahedron*, 2000, **56**, 6151–6170.

40 P. Thordarson, *Chem. Soc. Rev.*, 2011, **40**, 1305–1323.

41 K. R. Dymock and G. J. Palenik, *Inorg. Chem.*, 1975, **14**, 1220–1222.

42 E. L. Muetterties and L. J. Guggenberger, *J. Am. Chem. Soc.*, 1974, **96**, 1748–1756.

43 A. W. Addison, T. N. Rao, J. Reedijk, J. van Rijn and G. C. Verschoor, *J. Chem. Soc., Dalton Trans.*, 1984, 1349–1356.

44 P. Comba, M. Enders, M. Großhauser, M. Hiller, D. Müller and H. Wadepohl, *Dalton Trans.*, 2017, **46**, 138–149.

45 S. R. Bayly, Z. Xu, B. O. Patrick, S. J. Rettig, M. Pink, R. C. Thompson and C. Orvig, *Inorg. Chem.*, 2003, **42**, 1576–1583.

46 N. Ahmed, C. Das, S. Vaidya, S. K. Langley, K. S. Murray and M. Shanmugam, *Chem.–Eur. J.*, 2014, **20**, 14235–14239.

47 V. Vieru, T. D. Pasatoiu, L. Ungur, E. Suturina, A. M. Madalan, C. Duhayon, J.-P. Sutter, M. Andruh and L. F. Chibotaru, *Inorg. Chem.*, 2016, **55**, 12158–12171.

48 N. Kondoh, Y. Shimizu, M. Kurihara, H. Sakiyama, M. Sakamato, Y. Nishida, Y. Sadaoka, M. Ohba and H. Okawa, *Bull. Chem. Soc. Jpn.*, 2003, **76**, 1007–1008.

49 T. Shiga, N. Ito, A. Hidaka, H. Ōkawa, S. Kitagawa and M. Ohba, *Inorg. Chem.*, 2007, **46**, 3492–3501.

50 S. Orita and T. Akitsu, *Open Chem.*, 2014, **1**, 1–14.

51 P. Pyykkö, *J. Phys. Chem. A*, 2015, **119**, 2326–2337.

52 P. Pyykkö and M. Atsumi, *Chem.–Eur. J.*, 2009, **15**, 186–197.

53 B. Cordero, V. Gómez, A. E. Platero-Prats, M. Revés, J. Echeverría, E. Cremades, F. Barragán and S. Alvarez, *Dalton Trans.*, 2008, 2832–2838.

54 L. Pauling, *J. Am. Chem. Soc.*, 1947, **69**, 542–553.

55 J. A. Hlina, J. R. Pankhurst, N. Kaltsoyannis and P. L. Arnold, *J. Am. Chem. Soc.*, 2016, **138**, 3333–3345.

56 F. Völcker, F. M. Muck, K. D. Vogiatzis, K. Fink and P. W. Roesky, *Chem. Commun.*, 2015, **51**, 11761–11764.

57 F. Völcker and P. W. Roesky, *Dalton Trans.*, 2016, **45**, 9429–9435.

58 T. R. O'Toole, J. N. Younathan, B. P. Sullivan and T. J. Meyer, *Inorg. Chem.*, 1989, **28**, 3923–3926.

59 I. Noviandri, K. N. Brown, D. S. Fleming, P. T. Gulyas, P. A. Lay, A. F. Masters and L. Phillips, *J. Phys. Chem. B*, 1999, **103**, 6713–6722.

60 (*a*) L. J. Clouston, R. B. Siedschlag, P. A. Rudd, N. Planas, S. Hu, A. D. Miller, L. Gagliardi and C. C. Lu, *J. Am. Chem. Soc.*, 2013, **135**, 13142–13148; (*b*) R. Cammarota, PhD thesis, University of Minnesota, 2018.

61 P. A. Rudd, S. Liu, L. Gagliardi, V. G. Young and C. C. Lu, *J. Am. Chem. Soc.*, 2011, **133**, 20724–20727.

62 J. P. Perdew, M. Ernzerhof and K. Burke, *J. Chem. Phys.*, 1996, **105**, 9982–9985.

63 S. Grimme, *J. Comput. Chem.*, 2006, **27**, 1787–1799.

64 S. Grimme, J. Antony, S. Ehrlich and H. Krieg, *J. Chem. Phys.*, 2010, **132**, 154104–154119.

65 B. O. Roos, P. R. Taylor and P. E. M. Siegbahn, *Chem. Phys.*, 1980, **48**, 157–173.

66 D. You, H. Yang, S. Sen and F. P. Gabbaï, *J. Am. Chem. Soc.*, 2018, **140**, 9644–9651.

67 B. R. Barnett, C. E. Moore, P. Chandrasekaran, S. Sproules, A. L. Rheingold, S. DeBeer and J. S. Figueroa, *Chem. Sci.*, 2015, **6**, 7169–7178.

68 T.-P. Lin and J. C. Peters, *J. Am. Chem. Soc.*, 2014, **136**, 13672–13683.

69 M. V. Vollmer, J. Xie, R. C. Cammarota, V. G. Young, E. Bill, L. Gagliardi and C. C. Lu, *Angew. Chem., Int. Ed.*, 2018, **57**, 7815–7819.

70 G. Aullón and S. Alvarez, *Inorg. Chem.*, 1996, **35**, 3137–3144.

71 P. J. Desrosiers, L. Cai, Z. Lin, R. Richards and J. Halpern, *J. Am. Chem. Soc.*, 1991, **113**, 4173–4184.

72 T. J. Mooibroek, E. C. M. Wenker, W. Smit, I. Mutikainen, M. Lutz and E. Bouwman, *Inorg. Chem.*, 2013, **52**, 8190–8201.

73 K. V. Vasudevan, B. L. Scott and S. K. Hanson, *Eur. J. Inorg. Chem.*, 2012, **2012**, 4898–4906.

74 I. M. Angulo and E. Bouwman, *J. Mol. Catal. A: Chem.*, 2001, **175**, 65–72.

75 J. Camacho-Bunquin, M. J. Ferguson and J. M. Stryker, *J. Am. Chem. Soc.*, 2013, **135**, 5537–5540.

76 I. M. Angulo, A. M. Kluwer and E. Bouwman, *Chem. Commun.*, 1998, 2689–2690.

77 Y. Wang, A. Kostenko, S. Yao and M. Driess, *J. Am. Chem. Soc.*, 2017, **139**, 13499–13506.

78 J. Wu, J. W. Faller, N. Hazari and T. J. Schmeier, *Organometallics*, 2012, **31**, 806–809.

79 N. G. Léonard and P. J. Chirik, *ACS Catal.*, 2018, **8**, 342–348.

80 P. L. Holland, *Dalton Trans.*, 2010, **39**, 5415–5425.